

Robustness Analysis of Stator Voltage Vector Direct Torque Control for Induction Motor

Aleksandar Ž. Rakić, Slobodan N. Vukosavić

University of Belgrade, School of Electrical Engineering
Belgrade, Serbia
rakic@etf.rs, boban@etf.rs

Petar R. Matić

University of Banja Luka, School of Electrical Engineering
Banja Luka, Republic of Srpska, Bosnia and Herzegovina
per@etfbl.net

Abstract—In this paper, robustness analysis of Stator Voltage Vector Direct Torque Control (SVV DTC) for induction motor (IM) against rotor time-constant uncertainty is performed using modern linear robust theory. Appropriate structured robust model of the plant is derived and frequency domain setup is proposed to test robust stability, as well as nominal and robust performance in the sense of closed-loop set-point tracking. Results of the analysis confirm full stability robustness. Desired nominal and robust performance is confirmed in the motor field-weakening regime, while performance degradation is found at low motor speed.

Keywords: Induction Motors, Field Weakening, Torque Control, Robust Stability, Robust Performance.

I. INTRODUCTION

In IM drives, torque and flux are coupled. Attempts has been made [1–6] to achieve and verify high performance control in the field weakening regime, using stator voltage angle as the only independent control variable. Generalization of this approach is proposed in [7] and named Stator Voltage Vector Direct Torque Control (SVV DTC). Algorithm simultaneously controls motor torque and rotor flux by using stator voltage angle and amplitude in the base speed region, while the voltage angle only is used in the field weakening region. Robustness of the SVV DTC solution against rotor time-constant uncertainty is not presented in [7] and it is the subject of this paper.

The paper is organized as follows. In Section II appropriate robust model of the regulated plant is derived. Nonlinear state-space model of IM is presented, as well as linearized model, model approximation and essential characteristics of decoupled control from [7]. Also, structured robust model of the plant is derived to fit the modern linear robust theory [8-9]. Robustness analysis in the frequency domain is presented in Section III. Frequency setup is proposed to test closed-loop robustness properties. Robust stability, nominal performance, and robust performance are analyzed and results are discussed in separate subsections. Conclusion is given in Section IV.

II. ROBUST MODELING

A. Nonlinear Model of Induction Motor

The nonlinear state-space model of the IM, in normalized (per-unit [p.u]) values, is given as follows:

$$\frac{d\Psi}{dt} = \mathbf{A}(\omega_e, s)\Psi + \omega_b [U \ 0 \ 0 \ 0]^T, \quad (1)$$

$$\mathbf{A}(\omega_e, s) = \omega_b \begin{bmatrix} 1/T'_s & \omega_e & k_r/T'_s & 0 \\ -\omega_e & -1/T'_s & 0 & k_r/T'_s \\ k_s/T'_r & 0 & -1/T'_r & s\omega_e \\ 0 & k_s/T'_r & -s\omega_e & -1/T'_r \end{bmatrix}, \quad (2)$$

$$t_e = \frac{1}{\sigma l_s} (\Psi_D \Psi_q - \Psi_Q \Psi_d). \quad (3)$$

where the state vector consists of stator and rotor fluxes:

$$\Psi = [\Psi_d \ \Psi_q \ \Psi_D \ \Psi_Q]^T. \quad (4)$$

The model assumes: synchronous frequency ω_e and voltage modulus U as the control variables, motor torque t_e and rotor flux modulus $\Psi_r = \sqrt{\Psi_D^2 + \Psi_Q^2}$ as the output variables, mechanical transients much slower than electrical ones, and the reference frame aligned with stator voltage:

$$u_{sd} = U, \ u_{sq} = 0. \quad (5)$$

In the model (1) – (4), s stands for relative motor slip, ω_b is base speed, R_s and R_r are stator and rotor resistance, L_s and L_r are stator and rotor self-inductances, M is mutual inductance, $k_s = M/L_s$ and $k_r = M/L_r$ are stator and rotor coupling coefficients, $T'_s = \omega_b \sigma L_s / R_s$ and $T'_r = \omega_b \sigma L_r / R_r$ are stator and rotor transient time constants in [p.u], $\sigma = 1 - M^2 / L_s L_r$ is leakage coefficient and l_s is stator inductance in [p.u].

B. Linearized Model

For the given operation regime $(\omega_e, s) = (\omega_e^0, s^0)$, established by stationary control voltage $U = U^0$, nonlinear model (1) – (3) gives steady-state vector of fluxes

$$\Psi^0(\omega_e^0, s^0) = -\mathbf{A}^{-1}(\omega_e^0, s^0) \omega_b [U^0 \ 0 \ 0 \ 0]^T. \quad (6)$$

Assuming increment of the control vector

$$\mathbf{u} = [\omega_e - \omega_e^0 \quad U - U^0]^T \quad (7)$$

produces increments of the state vector and output vector, respectively:

$$\mathbf{x} = \Psi - \Psi^0, \quad (8)$$

$$\mathbf{y} = [t_e - t_e^0 \quad \Psi_r - \Psi_r^0]^T, \quad (9)$$

linearized model is found in [7] as:

$$\dot{\mathbf{x}} = \mathbf{A}(\omega_e^0, s^0) \mathbf{x} + \mathbf{B}(\omega_e^0, s^0) \mathbf{u}, \quad \mathbf{y} = \mathbf{C}(\omega_e^0, s^0) \mathbf{x}, \quad (10)$$

where $\mathbf{A}(\omega_e^0, s^0)$ is given in (2) for $(\omega_e, s) = (\omega_e^0, s^0)$, and

$$\mathbf{B}(\omega_e^0, s^0) = \omega_b \begin{bmatrix} \Psi_q^0 & -\Psi_d^0 & \Psi_\varrho^0 & -\Psi_D^0 \\ 1 & 0 & 0 & 0 \end{bmatrix}^T, \quad (11)$$

$$\mathbf{C}(\omega_e^0, s^0) = \begin{bmatrix} -\frac{k_r}{\sigma l_s} \Psi_\varrho^0 & \frac{k_r}{\sigma l_s} \Psi_D^0 & \frac{k_r}{\sigma l_s} \Psi_q^0 & -\frac{k_r}{\sigma l_s} \Psi_d^0 \\ 0 & 0 & \frac{\Psi_D^0}{\Psi_r^0} & \frac{\Psi_\varrho^0}{\Psi_r^0} \end{bmatrix}. \quad (12)$$

C. Linearized Model Approximation and Decoupling Control

From the state-space linearized model (10)-(12), transfer function matrix can be found as

$$G(p) = C(pI - A)^{-1} B. \quad (13)$$

Since analytic solution for the transfer function out of state-space representation (10)–(12) was found [7] to be rather complicated, in that paper approximated transfer function matrix was adopted, in which the static gain matrix and common pair of complex-conjugate rotor-related poles have been included as the functions of operation regime (ω_e^0, s^0) . It was also shown in [7] that nonlinear static decoupler achieves static gain decoupling and effective decoupled plant model was adopted in the form

$$G_{dc}(p) = \frac{1}{p^2 / \omega_{nr}^2 + (2\zeta / \omega_{nr}) p + 1} \begin{bmatrix} 1 & 0 \\ 0 & 1 \end{bmatrix}, \quad (14)$$

where natural frequency and relative damping ratio were adopted for the unloaded motor and they were found to be, respectively:

$$\omega_{nr} = \frac{\omega_b}{T_r} \frac{\sqrt{(\omega_e^0 T_s')^2 + (1 - k_s k_r)^2}}{\sqrt{(\omega_e^0 T_s')^2 + 1}}, \quad (15)$$

$$\zeta_r = \frac{(\omega_e^0 T_s')^2 + 1 - k_s k_r}{\sqrt{(\omega_e^0 T_s')^2 + 1} \sqrt{(\omega_e^0 T_s')^2 + (1 - k_s k_r)^2}}, \quad (16)$$

Since both torque and flux channel of decoupled plant have the same transfer function, torque and flux controllers were proposed with the same proportional-integral structure and the same parameters:

$$K(p) = K_{t_e}(p) = K_{\Psi_r}(p) = K_i \frac{p / \omega_z + 1}{p}, \quad (17)$$

where K_i is controller's integral gain and ω_z is frequency of the controller's zero, respectively:

$$K_i = \omega_0 = \frac{\omega_b}{10 T_r}, \quad (18)$$

$$\omega_z = \frac{\omega_b}{2 T_r} \cdot \min(1, 1 - k_s k_r + 2|\omega_e^0|). \quad (19)$$

Desired closed loop properties for both channels of control were: bandwidth ω_0 – a decade before the limit frequency of rotor poles, and phase margin of 90 deg.

D. Robust Model

In order to evaluate robustness of the control proposed in [7] to rotor time-constant uncertainty, appropriate robust model of each channel transfer function is to be derived. Rotor-related poles' positions, but without the unloaded motor assumption, were also found in [7]:

$$p_{r1,2}(\omega_e^0, s^0) = -\frac{\omega_b}{T_r} \frac{1 - k_s k_r + (\omega_e^0 T_s')^2}{1 + (\omega_e^0 T_s')^2} \pm j \omega_b \omega_e^0 \left(s^0 + \frac{k_s k_r T_s' / T_r'}{1 + (\omega_e^0 T_s')^2} \right). \quad (20)$$

Natural frequency of rotor-poles is given by

$$|p_{r1,2}(\omega_e^0, s^0)| = k_0 + \frac{1}{T_r} \left(k_1 + \frac{1}{T_r} k_2 \right), \quad (21)$$

where:

$$k_0 = (\omega_b s^0 \omega_e^0)^2, \quad (22)$$

$$k_1 = 2k_s k_r T_s' s^0 (\omega_b \omega_e^0)^2 / \left(1 + (T_s' \omega_e^0)^2 \right), \quad (23)$$

$$k_2 = \omega_b^2 \left((1 - k_s k_r)^2 + (T_s' \omega_e^0)^2 \right) / \left(1 + (T_s' \omega_e^0)^2 \right). \quad (24)$$

Introducing the fourth parameter

$$k_4 = 2 \operatorname{Re}\{p_{1,2}\} \cdot T_r' = -2\omega_b \frac{1 - k_s k_r + (\omega_e^0 T_s')^2}{1 + (\omega_e^0 T_s')^2}, \quad (25)$$

channel transfer function

$$G_c(s) = \frac{1}{\left(\frac{p}{p_1} - 1\right)\left(\frac{p}{p_2} - 1\right)} = \frac{1}{\frac{p^2}{|p_{1,2}|^2} + \frac{2 \operatorname{Re}\{p_{1,2}\}}{|p_{1,2}|^2} p + 1} \quad (26)$$

can be described by the block diagram given in Fig. 1.

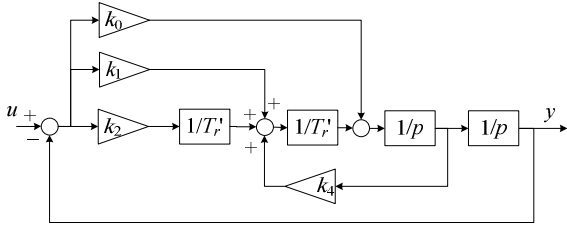


Figure 1. Structural block diagram of the channel transfer function.

However, the actual value of the rotor time-constant T_r' is highly dependent, mainly but not only, on the IM working temperature. It can deviate significantly from its presumed nominal value even during normal operation of the motor. Therefore, robust IM model should incorporate adequate information on the rotor time-constant uncertainty.

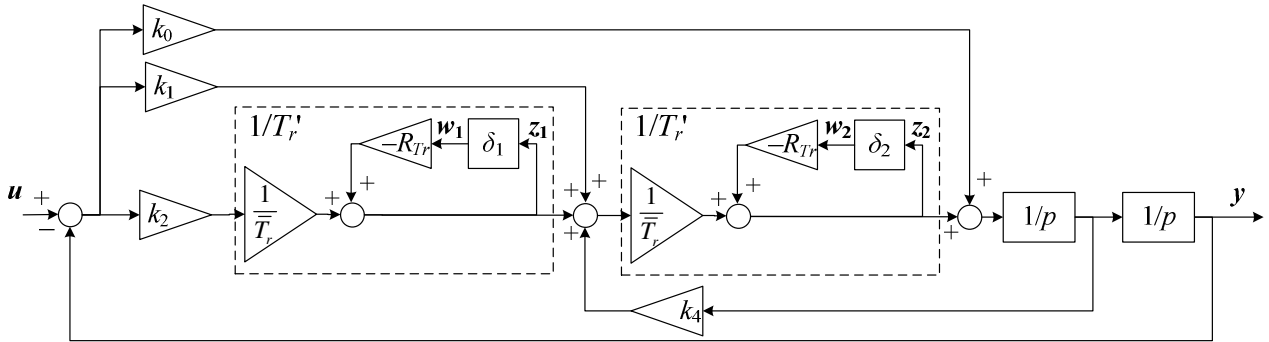


Figure 2. Structural block diagram of the channel transfer function with the uncertainty description of the rotor time constant

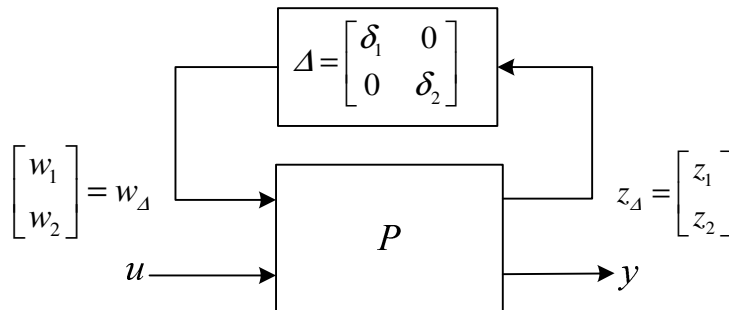


Figure 3. Generic model with structured uncertainty

Assuming the rotor time-constant T_r' is uncertain, but lies within the percentage range R_{Tr} of the nominal value \bar{T}_r' , the appropriate description of the uncertainty is

$$T_r' = \bar{T}_r' (1 + R_{Tr} \delta), \quad (27)$$

where δ is the unknown real value in the normalized unity range

$$|\delta| \leq 1. \quad (28)$$

Block diagram of the channel transfer function with incorporated uncertainty description (27) is given in Fig. 2. It is equivalent to the generic block diagram of the structured robust model in Fig. 3, when the known part P of the plant is given by the state-space matrices, respectively:

$$\mathbf{A}_p = \begin{bmatrix} 0 & 1 \\ -k_0 - (k_1 + k_2 / \bar{T}_r) / \bar{T}_r & k_4 / \bar{T}_r \end{bmatrix}, \quad (29)$$

$$\mathbf{B}_p = \begin{bmatrix} 0 & 0 & 0 \\ -R_{Tr} / \bar{T}_r & -R_{Tr} & k_0 + (k_1 + k_2 / \bar{T}_r) / \bar{T}_r \end{bmatrix}, \quad (30)$$

$$\mathbf{C}_p = \begin{bmatrix} -k_2 / \bar{T}_r & -(k_1 + k_2 / \bar{T}_r) / \bar{T}_r & 1 \\ 0 & k_4 / \bar{T}_r & 0 \end{bmatrix}^T, \quad (31)$$

$$\mathbf{D}_p = \begin{bmatrix} -R_{Tr} & 0 & k_2 / \bar{T}_r \\ -R_{Tr} / \bar{T}_r & -R_{Tr} & (k_1 + k_2 / \bar{T}_r) / \bar{T}_r \\ 0 & 0 & 0 \end{bmatrix}^T. \quad (32)$$

III. CLOSED-LOOP ROBUSTNESS ANALYSIS

A. Frequency Domain Setup

The robustness analysis setup is presented in Fig. 4.

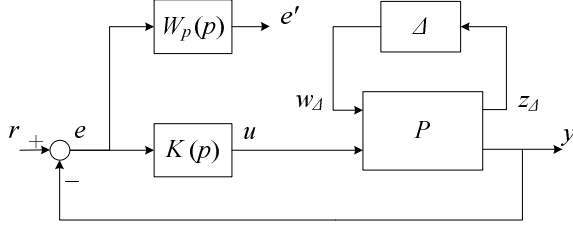


Figure 4. Block diagram of robust reference tracking control setup.

Following signals are denoted: r – the reference (set point) signal, $e = r - y$ is the error in reference tracking, e' – the performance weighted error, u – the control signal, w_Δ – uncertainty output, and z_Δ – uncertainty input.

Relevant transfer functions are: $K(p)$ – the controller (17)–(19), P – the known part (29)–(32) of the uncertain plant, Δ – an unknown uncertainty of modeling, and $W_p(p)$ – the performance weighting function.

The performance weighting function is adopted in the form

$$W_p(p) = \frac{1}{M_s} \frac{p + M_s^* \omega_0^*}{p}, \quad (33)$$

with the choice of parameters ensuring adequate reference-tracking performance evaluation: desired closed-loop bandwidth (a tenth of rotor poles' limit frequency)

$$\omega_0^* = \frac{\omega_b / T_r'}{10}, \quad (35)$$

and tight bound for maximum sensitivity [8–9]

$$M_s^* = 1.2. \quad (34)$$

If known part P of the plant is partitioned as

$$\begin{bmatrix} z_\Delta \\ y \end{bmatrix} = \begin{bmatrix} P_{11} & P_{12} \\ P_{21} & P_{22} \end{bmatrix} \begin{bmatrix} w_\Delta \\ u \end{bmatrix}, \quad (36)$$

relevant closed-loop transfer function matrices are:

$$N_{11} = P_{11} - P_{12}K(I + P_{22}K)^{-1}P_{21} \quad (\text{transfer } w_\Delta \rightarrow z_\Delta), \quad (37)$$

$$N_{21} = W_p(I + P_{22}K)^{-1}P_{21} \quad (\text{transfer } w_\Delta \rightarrow e'), \quad (38)$$

$$N_{12} = P_{12}K(I + P_{22}K)^{-1} \quad (\text{transfer } r \rightarrow z_\Delta), \quad (39)$$

$$N_{22} = W_p(I + P_{22}K)^{-1} \quad (\text{transfer } r \rightarrow e'), \quad (40)$$

and indexes of closed-loop robust stability, nominal performance, and robust performance are, respectively:

$$RS = \max_{\omega} \mu_\Delta(N_{11}(j\omega)), \quad (41)$$

$$NP = \max_{\omega} \bar{\sigma}(N_{22}(j\omega)), \quad (42)$$

$$RP = \max_{\omega} \mu_\Delta \left(\begin{bmatrix} N_{11}(j\omega) & N_{12}(j\omega) \\ N_{21}(j\omega) & N_{22}(j\omega) \end{bmatrix} \right), \quad (43)$$

where: $\bar{\sigma}(\cdot)$ is upper singular value, and $\mu_\Delta(\cdot)$ is structured singular value.

The closed-loop system has robust stability (it is stable for every perturbation of uncertain parameter Tr') if

$$RS < 1, \quad (44)$$

while nominal performance and robust performance are satisfied if, respectively:

$$NP < 1, \quad (45)$$

$$RP < 1. \quad (46)$$

Condition (44) is mandatory because $RS > 1$ means there is at least one perturbed value Tr' that makes closed-loop system unstable. Violation of condition (45) means the closed-loop system with *nominal plant* (nominal Tr') does not fulfill desired bandwidth (35) or/and maximum sensitivity (34). Violation of condition (46) means there is at least one perturbed value Tr' that makes closed-loop system not fulfilling desired bandwidth (35) or/and maximum sensitivity (34).

B. Nominal Performance Results

Nominal performance index NP (42) with the test motor (parameters given in Appendix) for increasing synchronous speed at different steady state slips is plotted in Fig. 5.

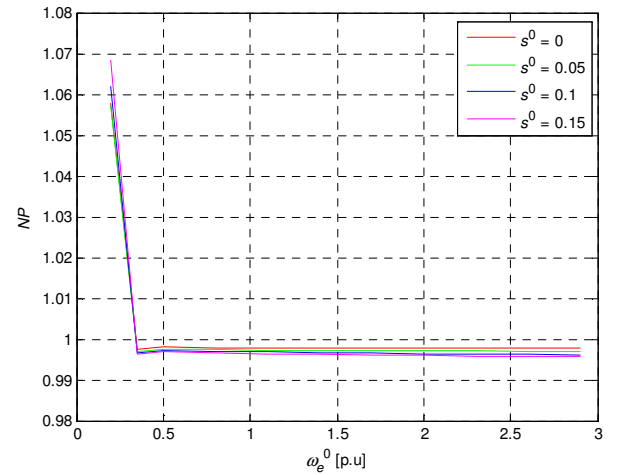


Figure 5. Nominal performance index NP .

It can be observed that nominal performance is not dependant the stationary motor slip s^0 , i.e. the motor load. Nominal performance is not fulfilled only at very low synchronous speeds since (45) not satisfied at $\omega_e^0 < 0.2$ p.u.

C. Robust Stability Results

For the test motor model with the uncertain rotor time-constant T_r' within the plus/minus percentage range

$$R_{Tr} = 99\% \quad (47)$$

of the nominal value \bar{T}_r' , robust stability index RS (41) is plotted in Fig. 6 for increasing synchronous speed at different steady state slips.

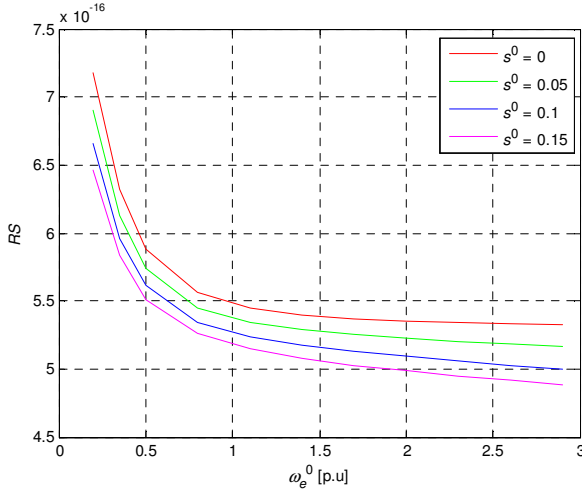


Figure 6. Robust stability index RS for uncertainty bound $R_{Tr} = 99\%$.

It can be observed that robust stability condition (44) is fulfilled for the full range of motor speeds and loads. Therefore, robust stability is achieved over the whole set of perturbed plants and in all operating regimes.

D. Robust Performance Results

Robust performance index RP (43) is plotted in Fig. 7 for the test motor model with the uncertain rotor time-constant T_r' within the plus/minus percentage range (47). It can be observed that robust performance condition (46) is not fulfilled for the unloaded motor ($s^0 = 0$) on the full range of motor speeds. However, this RP characteristic exceeds boundary value of 1 for less than 5% in the field-weakening regime, where the control schema performance is essential. Moreover, all “loaded” characteristics ($s^0 > 0$) achieve less than 5% RP degradation starting from the half of the nominal motor speed, and the fully achieve robust performance in the whole field-weakening area.

Robust performance degradation is further studied for tighter uncertainty bounds. In Figs. 8-9, robust performance index RP is plotted for uncertainty percentage ranges, respectively:

$$R_{Tr} = 80\% , \quad (48)$$

$$R_{Tr} = 50\% . \quad (49)$$

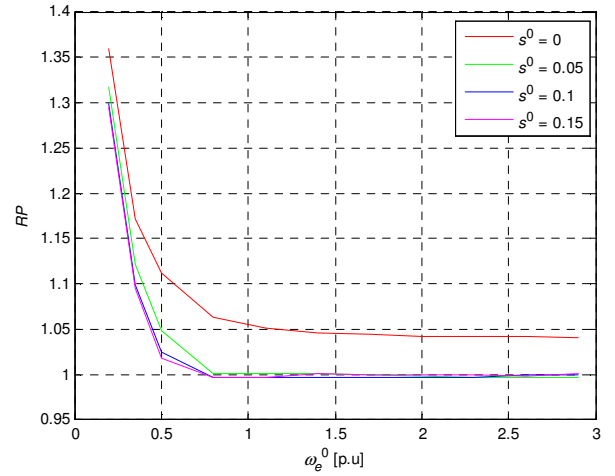


Figure 7. Robust performance index RP for uncertainty bound $R_{Tr} = 99\%$.

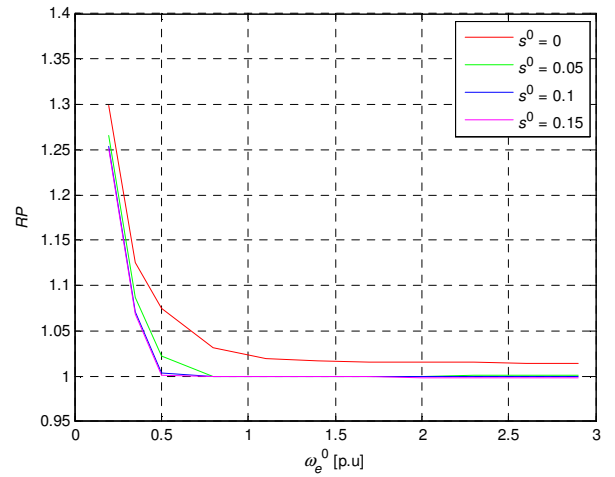


Figure 8. Robust performance index RP for uncertainty bound $R_{Tr} = 80\%$.

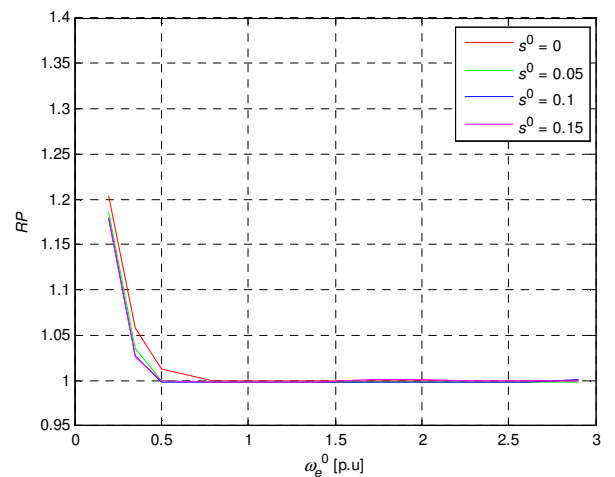


Figure 9. Robust performance index RP for uncertainty bound $R_{Tr} = 50\%$.

On both plots, robust performance is fully achieved in the whole field-weakening area, and breaches of robust performance bound are significant only up to the half of the nominal motor speed. Tighter uncertainty bound (48) enables full robust performance achievement for all “loaded” characteristics starting from $\omega_e^0 = 0.75$ p.u., while the “unloaded” characteristic exceeds unity bound on the whole speed range. Even tighter uncertainty bound (49) makes all the characteristic fully achieve robust performance starting from the speed $\omega_e^0 = 0.75$ p.u.

IV. CONCLUSION

In the paper robust control theory was utilized to verify robustness properties of the SVV DTC solution for IM control. Conducted robustness analysis provides evidence that closed-loop system will be stable both in base-speed and field-weakening regime, even with high uncertainty of estimated rotor time-constant.

Nominal and robust performance is proven to be fully achieved only in the field-weakening regime, while performance degradation is detected in the low-speed region. However, SVV DTC solution is intended for high-speed low-cost IM drives working in deep field weakening range, so base-speed performance is not essential.

Proposed analysis is conducted on the structured robust model of the decoupled plant’s channel transfer function. Further work could be directed toward more complex analysis, based on the original multivariable linear IM model, which could give deeper insight on achievable robust properties and potentially better control design.

APPENDIX

Motor data: 750W, 195V, 70Hz, $R_s = 10.8\Omega$, $R_r = 5.673\Omega$, $L_s = L_r = 0.552$ H, $L_m = 0.518$ H.

REFERENCES

- [1] P. Matic, A. Rakić, and S. Vukosavić, "Induction Motor Torque Control in Field Weakening by Voltage Angle Control," in Proc. 14th Int. Power Electronics and Motion Control Conf. (EPE/PEMC), Ohrid, Macedonia, Sep. 6–8, 2010, pp. T4-108–T4-115.
- [2] P. Matic, A. Rakić, and S. Vukosavić, "Direct Torque Control of Induction Motor in Field Weakening Based on Gain-Scheduling Approach," in Proc. 16th Int. Symp. Power Electronics (Ee 2011), Novi Sad, Serbia, Oct. 26–28, 2011.
- [3] A. Rakić, P. Matic, "Robust Modeling and Reference Tracking Control of Voltage Angle Controlled Induction Motor in Field Weakening Regime," in Proc. INDEL Conf., Banja Luka, Republic of Srpska - Bosnia and Herzegovina, Nov. 4–6, 2010, pp. 262-267.
- [4] P. Matic, I. Krčmar, A. Rakić, S. N. Vukosavić, "Improved Induction Motor Performance in the Field Weakening Based on the PI Controller Gain Sceduling (in Serbian)," in Proc. 10th Infoteh-Jahorina Conf., Jahorina, Republic of Srpska - Bosnia and Herzegovina, Mar. 16–18, 2011, Vol. 10, Ref. A-7, pp. 31-35.
- [5] A. Rakić, P. Matic, T. Petrović, "Robust Modeling and Gain-Scheduling Control of the Induction Motor in the Field Weakening Regime," in Proc. LV ETRAN Conf., Banja Vrućica-Teslić, Republic of Srpska - Bosnia and Herzegovina, Jun. 6-9, 2011, pp. AU4.5-1-4.
- [6] P. Matic, A. Rakić, S. N. Vukosavić, "Space Vector Induction Motor Model in Field Weakening (in Serbian)," in Proc. LV ETRAN Conf., Banja Vrućica-Teslić, Republic of Srpska - Bosnia and Herzegovina, Jun. 6-9, 2011, pp. EE1.5-1-4.
- [7] P. R. Matic, A. Ž. Rakić, and S. N. Vukosavić, "Stator Voltage Vector Direct Torque Control of Induction Machine," in Proc. 15th Int. Power Electronics and Motion Control Conf. (EPE/PEMC), Novi Sad, Serbia, Sep. 4–6, 2012.
- [8] S. Skogestad, I. Postlethwaite, Multivariable Feedback Control. England: John Willey & Sons, 1996.
- [9] K. Zhou, J. C. Doyle, K. Glover, Robust and Optimal Control. New Jersey: Prentice-Hall, 1996.